

Analyzing the macro and micro-scale response of an idealised granular material in direct shear test using 3D-DEM simulations and experimental investigations



Challenges from North to South
Des défis du Nord au Sud

Amirpour Harehdasht Samaneh, Mourad Karray & Mahmoud N. Hussien
Department of Civil Engineering, Faculty of Engineering, Sherbrooke University (QC), Canada
Mohamed Chekirad, Varvara Roubtsova
Institute de Research d'Hydro-Quebec (QC), Canada

ABSTRACT

This paper describes a promising virtual approach using SiGran (3D virtual laboratory for geotechnical applications) to observe the micro-scale behaviour of an idealized material in direct shear test, based on the discrete element methods (DEM). To validate the numerical simulations, a series of experimental tests were also carried out. The macro-scale results obtained from DEM simulations show good agreement with those of the laboratory tests. The micro scale results from numerical simulations also were derived showing the initiation of shear bands from the side boundaries toward the centre. When sample reached the peak state the distinct shear band along the middle plane developed and became more continuous and expansive during the post-peak. The micro scale results are in good agreements with previous study tried to evaluate the formation of shear band in two or three dimensional simulations.

RÉSUMÉ

Cet article décrit une approche virtuelle prometteuse en utilisant SiGran (laboratoire virtuel en 3D pour les applications géotechniques) pour observer le comportement à une micro-échelle d'un matériau idéal durant l'essai de cisaillement direct sur la base des méthodes d'éléments discrets (DEM). Pour valider les simulations numériques, une série d'essais de laboratoire a été effectuée. Les résultats à une macro-échelle obtenus à partir de simulations DEM montrent un bon accord avec ceux des essais de laboratoire. Les résultats à une micro-échelle obtenus montrent aussi l'initiation de bandes de cisaillement à partir des limites latérales vers le centre. Lorsque l'échantillon atteint le pic, une bande de cisaillement distincte le long du plan médian est développée et persiste davantage après le pic. Les résultats à une micro-échelle concordent avec les études réalisées dans le passé qui ont tenté d'évaluer la formation de la bande de cisaillement dans des simulations 2D ou 3D.

1 INTRODUCTION

The direct shear apparatus (DSA) is one of the most widely used devices for obtaining effective stress shear strength parameters for soil since approximately 150 years ago. Due to some criticisms of the direct shear test including non-uniformity of stresses and strains applied to the sample (Terzaghi and Peck, 1948, Hvorslev 1960), and ambiguity in interpreting shear strength parameters at failure (Morgenstern & Tchalenko, 1967), the direct shear test fell out of favor in the geotechnical community for some time. However, in recent years the direct shear test has seen resurgence in its use, primarily because tests are simple and typically of lower cost than other geotechnical tests.

Over the past decades, some experimental observations (Dyer and Milligan 1984, Jewell and Wroth 1987) and numerical simulations (Pottes et al 1987, Zang and Thornton 2007, Cho et al. 2008) have been done to observe the micro-scale behaviour and formation of stress and strains within the direct shear box during shear. However, accuracy limitations of experimental devices and difficulty in extraction of micromechanical data, as well as the need for expensive equipment are the major hindering factors in performing laboratory experiments to

understand the micro-mechanics of granular material. On the other hand, using simulations one can easily generate plenty of data for studying the effect of various parameters. For this purpose, numerical models are trying to provide unique insight into the micro-mechanics of granular shear deformation and offer great potential for bridging the gap between laboratory conditions and geotechnical engineering practice. Since the pioneering work of Cundall and Strack (1979), the DEM has been widely accepted to analyze the mechanical characteristics of granular material.

DEM simulation can treat the granular material as an assembly of particles that interact via a contact logic and can offer a thorough perspective of the response at the particulate level as well as the overall behaviors. While there are numerous publications describing the potential of DEM, only a small number of studies in the geotechnical field have been validated by experimental results.

The aim of paper is to use DEM simulations capturing the micro and macro-scale response of the sample's behavior made up of glass beads in direct shear. For this purpose, SiGran (3D virtual laboratory for geotechnical applications, IREQ) is employed. The quantitative validation of the DEM model is attempted by relating a

series of experimental tests to equivalent DEM simulations. Direct shear test simulation is part of a large research program oriented toward the development of a virtual laboratory (SiGran) dedicated to the study of a number of geotechnical phenomena (Roubtsova et al. 2011, Roubtsova et al. 2015).

In addition, the latter section of the paper shows how the simulations also enable visualization of particle behavior at particle level in 3D. This leads to additional evidence that justifies the use of the DSA data at peak state and shows why results are comparable to simple shear within the shear band. Coupling the results at the macro-scale of direct shear simulation using SiGran with experimental tests and comparing with earlier DEM studies also allow the authors to make more confident interpretation of shear strength parameters, especially at failure stage. In condition of having the minor non-coaxiality and uniformity of stresses and strains at peak states, the boundary measurements made on the direct shear apparatus are valid and suitable for determining strength and volume change behaviour of granular material.

2 PHYSICAL DIRECT SHEAR TESTS

2.1 Material Properties

The Whitehouse polydisperse standard having the range sizes of 500-2000 μm was used to perform the tests. The Whitehouse polydisperse reference standards, which are typically spherical glass beads with a known distribution, are originally commissioned by the European Community Bureau of Reference (BCR). The particle size distribution, technical, and physical properties of selected polydisperse standard, using electroformed sieve analysis and microscopy method, is shown in Table 1.

Table 1. Properties of Whitehouse polydisperse standard

Reference Size (μm)	Size at Fixed Percentiles (μm)				
	10	25	50	75	90
500-2000 (+/-)	691 6	8538 8	1010 11	1248 24	1534 42
	Young Modulus N/mm^2				6.89×10^4
Technical Prop.	Rigidity Modulus N/mm^2				2.96×10^4
	Poisson ratio				0.21
Physical Prop.	Specific Gravity gr/cm^3				2.43-2.49

2.2 Experimental Test Apparatus

The direct shear test apparatus used in this study consists of a metal box with a square cross-section (55 mm wide), divided horizontally into two halves. During the tests, the lower section of the box was moved forward at a constant velocity of 0.0051 mm/s while the upper part was restrained against horizontal movement. The vertical load

was applied to the center of the floating top platen on the shear box using a system of an air compressor attached to a lever. The lower section and vertical displacement was measured by the transducers placed respectively on the center of the top platen.

The tilting of the top platen and the upper half of the box, and the collapsing the material at the edges constitute possible sources of unwanted effects and assist progressive failure mechanism, were prohibited in current tests, using a supplementary membrane.

Three direct shear box tests were performed at different normal pressures of 50, 200 and 400 kPa. The samples were prepared and sheared in dry conditions. Each test sample was prepared in the shear box in three layers of equal thickness. Dry mixtures were carefully laid down in the shear box using a spoon to prevent particle segregation.

3 DEM SIMULATIONS

The Discrete Element Method describes the motion of assemblies of particles and it is widely used as a mathematical tool to study the behavior of particle assemblages. This tool is based on Newton's second law for the interaction of particles. An explicit time stepping scheme is used for integration in time. The behavior of the particle assembly under external loading can be described at a time step using information from the previous time step. This information includes the dimension of each particle, its relative position to adjacent particles and the relative velocities (displacement and rotation) with neighboring particles. The contact forces acting on a particle are calculated from this data and the accelerations, velocities, and position at new time step determined. The concept of the interactive forces between particles is illustrated in Figure 1.

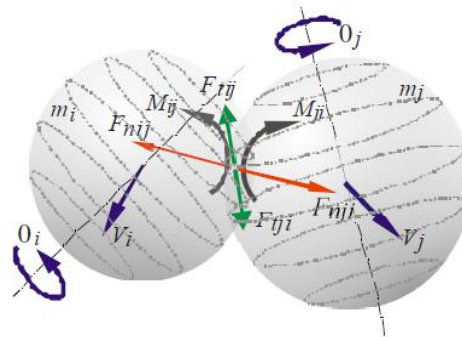


Figure 1. Interactive forces between two particles

This performed simulations cannot be regarded as quasi-static because the kinetic energy of translation and rotation are not neglected. This approach provides a very promising basis for building up constitutive equations for granular assemblies. The fundamental equations of motion for the i^{th} particle are as follows (the subscript j refers to the j^{th} neighboring particle, and k is the number of neighboring particles):

$$m_i \frac{d\bar{V}_i}{dt} = m_i \bar{g} + \sum_{j=1}^k (\bar{F}_{cn,ij} + \bar{F}_{dn,ij} + \bar{F}_{ct,ij} + \bar{F}_{dt,ij}) + \bar{F}_{ft} \quad [1]$$

$$I_i \frac{d\bar{\omega}_i}{dt} = \sum_{j=1}^k (\bar{T}_{ij} + \bar{M}_{ij}) + \bar{M}_{ft} \quad [2]$$

Where:

m_i and I_i are the mass (kg) and moment of inertia (kg.m²) of particle i respectively.

\bar{V}_i and $\bar{\omega}_i$ are the transitional and rotational velocities of particle i.

$$F_{cn,ij} = -K_n \delta_n^{3/2} \bar{n} \quad [3]$$

$F_{dn,ij} = -C_n \bar{V}_{n,ij}$ and $F_{dt,ij} = -C_t \bar{V}_{t,ij}$ are the normal and tangential damping forces (N) respectively.

$$\frac{d\bar{F}_{ct,ij}}{d\delta_t} = -K_t \text{ is the tangential force of contact (N).}$$

This force is limited by the coulomb's law $|F_{ct,ij}| \leq \mu_s F_{cn,ij}$.

$$\bar{T}_{ij} = R_i (\bar{F}_{ct,ij} + \bar{F}_{dt,ij}) \text{ is the rolling torque (N.m).}$$

$$\bar{M}_{ij} = -\mu_r |F_{cn,ij}| \frac{\omega_i}{|\omega_i|} \text{ is the friction torque (N.m).}$$

$$K_n = \frac{4}{3} E^* \sqrt{R^*}, C_n = 2\sqrt{m^* K_n} \quad [4]$$

$$K_t = 2\sqrt{R\delta_n} \left(\frac{G_i}{2-\nu_i} + \frac{G_j}{2-\nu_j} \right), C_t = K_n \sqrt{\frac{K_t}{K_n}} \quad [5]$$

δ_n and δ_t are the normal and tangential contact displacement respectively;

$$\frac{1}{E^*} = \frac{1-\nu_i^2}{E_i} + \frac{1-\nu_j^2}{E_j} \text{ and } \frac{1}{R^*} = \frac{1}{|R_i|} + \frac{1}{|R_j|} \quad [6]$$

Where E is Young's modulus (Pa), ν is Poisson ratio, R_i is the particle radius (m), and μ_s, μ_r are the sliding and rolling (m) friction coefficient respectively.

In addition, the SiGran code follows the conservation energy principle, allowing one to analyze energy transformations for a variety of processes such as the direct shear test.

3.1 Calibration

DEM models must be calibrated such that the assigned micro-parameters in the models produce the desired macro- properties of the material being simulated. Here, calibration is first done using the reported characteristics of the deformed sample in direct shear.

The virtual sample was generated by placing the particles randomly into the shear box and considering their interaction under the force of gravity. Following this step vertical stress was applied and the system allowed to come to equilibrium. Vertical pressure was applied as a small displacement of the top boundary. This displacement must be sufficient to stabilize a vertical force after a perturbation of particles at each time step and small enough to preserve the stability of calculation (Equation 7).

$$\delta_v = -1.10^{-3} d_{min} (S_r - S_t) / S_r \quad [7]$$

Where:

δ_v is the displacement of that top wall

d_{min} is the diameter of the smallest particle

S_r is the required vertical stress (Pa)

S_t is the current vertical stress (Pa)

The dimension of the sample is 55 mmx 55 mm, and the height of the low part is 10 mm. The mechanical properties of the particles in simulations are the same as those used for the physical direct shear tests (Table 1). All the parameters used in numerical simulations are summarized in Table 2.

Table 2. Input parameters for DEM simulations

Parameters	Value
Density	2450 kg/m ³
Number of Particles	102248
Particle/ Wall friction	0.3
Particle/ Particle friction	0.2
Rolling Friction	5.10 ⁻³ mm

3.2 Calibration results

Three normal stress magnitude of 50, 200 and 400 kPa were simulated to cover the range of normal stresses as reported for the laboratory tests. Figure 2 and Table 3, shows the direct shear SiGran simulation results when compared to the laboratory tests. To facilitate the comparison of the SiGran simulations and the laboratory tests, for these macro-scale results the shear and normal stresses calculated from the measured boundary forces and presented with the laboratory results as a function of shear displacement. The stresses obtained from the SiGran simulations exhibited some fluctuations, however, they did not affect the overall response of the sample during shear and are quite small in magnitude. The peak friction angle obtained from the failure envelopes for

numerical simulations is found to be 6% less than that of the laboratory tests (Figure 3).

Table 3. Summary of numerical and experimental results

Test Identification	τ_{max}/σ_n	ϕ'_{max} ($^{\circ}$)	Ψ_{max} ($^{\circ}$)	ϕ'_{cv} ($^{\circ}$)
50 kPa- Exp.	0.65	32.96	9.97	28.23
50 kPa- Num.	0.71	35.46	10.57	27.06
200 kPa- Exp.	0.58	30.14	6.08	26.56
200 kPa- Num.	0.60	31.08	9.36	25.54
400 kPa- Exp.	0.57	29.66	5.92	25.96
400 kPa- Num.	0.53	28.04	9.15	24.21

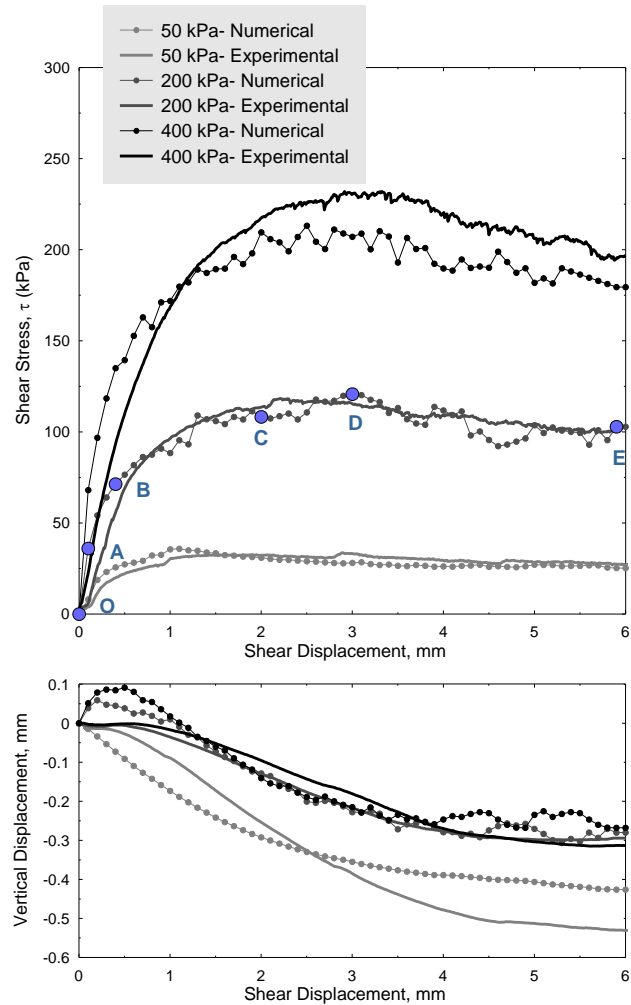


Figure 2. Stress-strain curves of numerical simulation and experimental tests

By reference to the Table 3, it can be observed that the ratio of maximum shear stress to normal stress decreases slightly with increasing normal stress for both laboratory tests and numerical simulations. This reduction in the stress ratio with increasing normal stress is the consequence of the dilation suppression during shear,

however the amount of dilation angles obtained from the simulations differ from the trend observed in the laboratory tests.

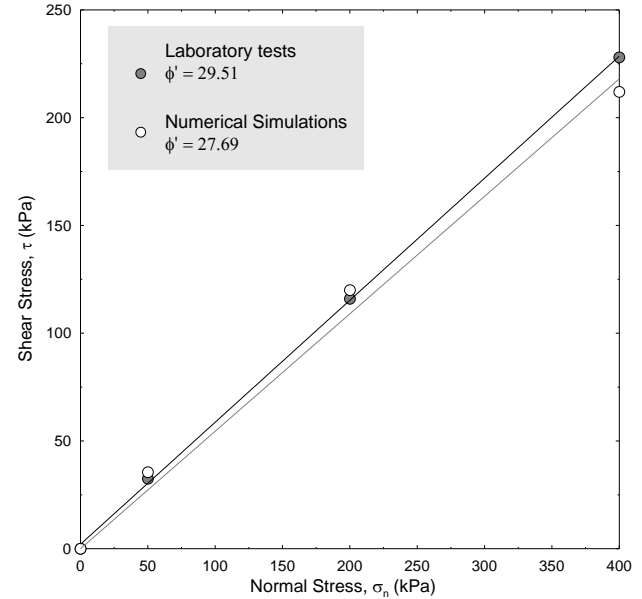
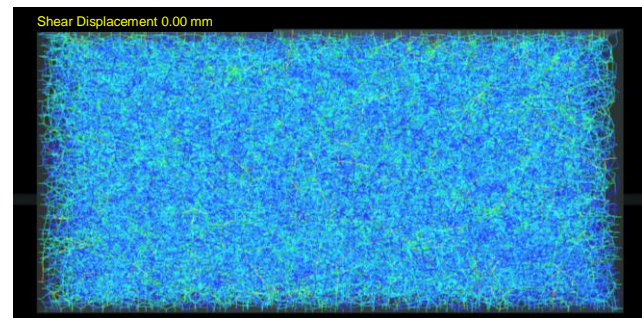


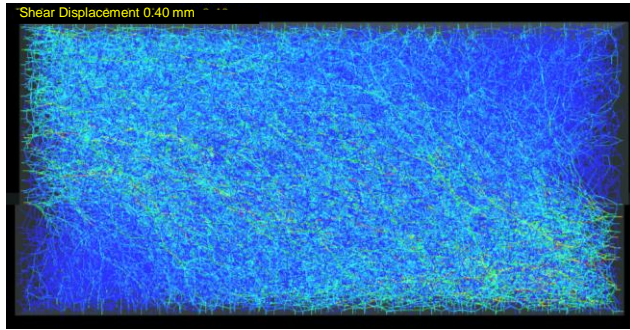
Figure 3. Failure envelopes for laboratory tests and numerical simulation

3.3 Force Transmission

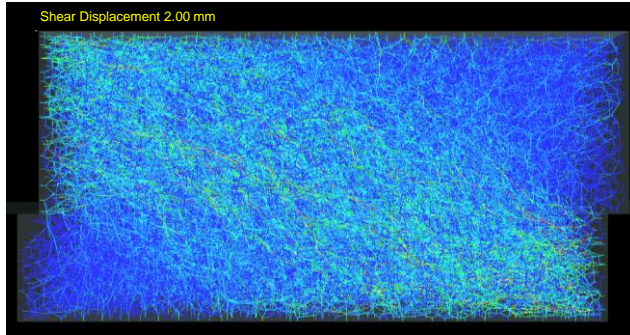
The force transmission through the system of particles, at three points of O, B, and C (Figure 2) from start of shearing until reaching the peak, for normal stress of 200 kPa are shown in Figure 4. Each line is drawn between the centres of two particles in contact with each other. The magnitudes of the forces increase by changing the colors from blue to red. It is clear from the Figure 4a that the distribution of forces before shearing, point O, is isotropic inside the sample. At first stage of shearing, point B, large contact forces start to develop towards the centre of the sample (Figure 4b), until the sample reaches the maximum shear strength at point C. At this point forces are partially influenced by the top and bottom boundaries, concentrate in the upper right and lower left corners and only small forces are transmitted to the other two vertical end walls. Consequently, the strong force transmission pathways are inclined as they pass through the shear zone at the mid-height of the sample (Figure 4c).



(a)



(b)



(c)

Figure 4. Contact forces network at three points of A, B, and C for sample under normal stress of 200 kPa

In Addition, the heterogeneity of force transmission pattern decreases by approaching the shearing at constant volume (Figure 5).

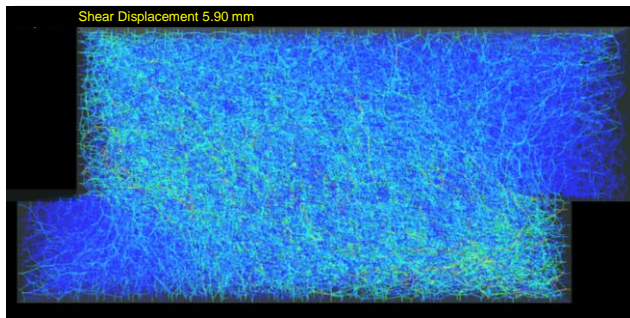
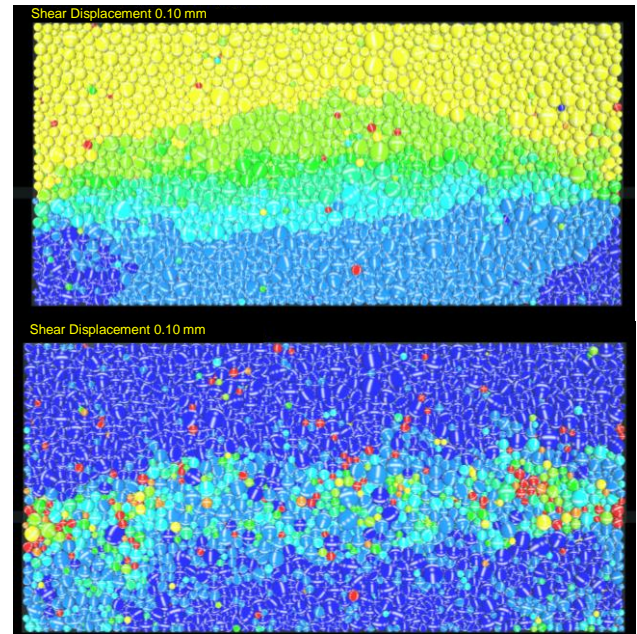


Figure 5. Contact forces network at point E, at the end of shearing

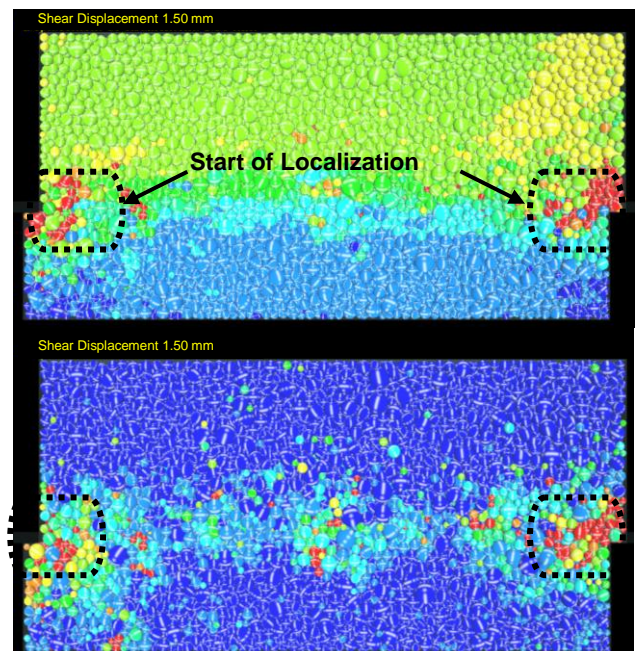
Comparing the shear forces of simulations at three different normal stresses reveals that the chain of strong forces appear more pronounced in samples by increasing the normal stress, however the main orientation of the contact forces are the same for three tests and transmitted diagonally across the sample. The force transmission pattern correlate very well with other direct shear numerical studies (Zang and Thornton 2007, Cho et al. 2008) and experimental works (Dyer and Milligan, 1984).

3.4 Velocities and Energies during Shearing

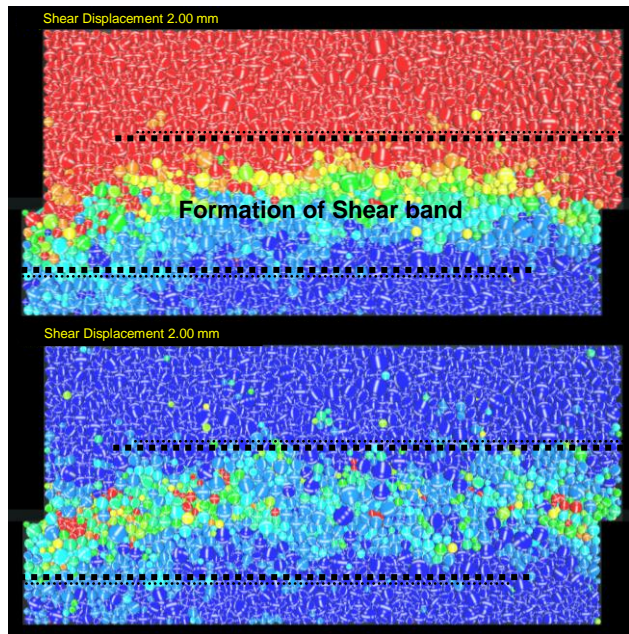
Figure 6 which presenting the snapshots of the particles transitional and rotational velocities at successive steps, gives a clear visualization of the strain localization inside the box during shear under normal stress of 200 kPa. The magnitudes of the velocities increase by changing the colors of particles from blue to red in the images. It should be noted that in Figure 6a the resolution of rotational velocities is 2.5 times greater than that used for Figure 5.b-d, in order to visualize the formation of shear band clearly at all stages.



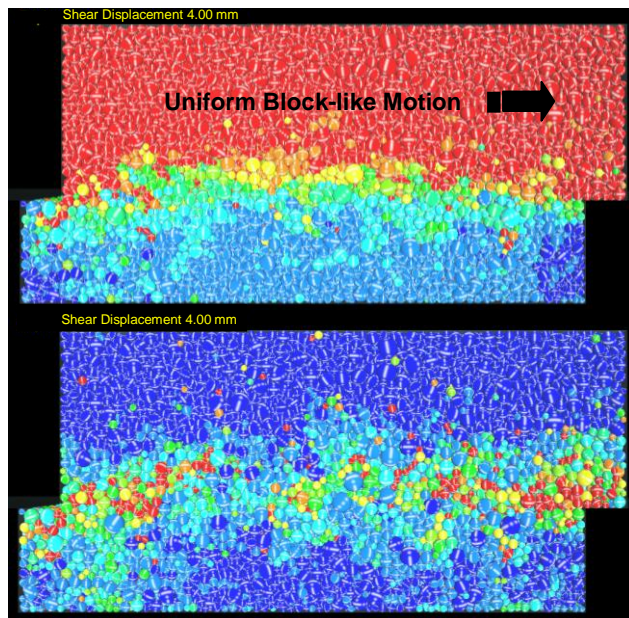
(a)



(b)



(c)



(d)

Figure 6. Evolution of transitional and rotational velocities during shearing (a) onset of dilation (b) 50% of peak (c) peak (d) post-peak

During the stage A to B, before dilation, transitional velocity gradients appears at the mid-height and towards the top and bottom edges, but no strain localization is revealed (Figure 6a). Small rotational velocities also observed through the sample at this stage (Figure 6a).

During the stage B to C (Figure 6b), owing to the boundary constraint, strain localization begins at the two lateral boundaries. As shearing proceeds, the shear zone extends slowly toward the middle of the box from the

boundaries. At the pre-peak state the shear band starts to extend over the length of the middle plane

The image of transitional velocities at the peak strength (stage C to D), shows the gradient of transitional velocity of particles become quite erratic by around the mid-height Figure 6c, where the high particles rotation become highly concentrated, as shown in Figure 6c. At this stage a distinct shear band has formed, which becomes more continuous and expansive with post-peak strain-softening.

After this stage the uniform transitional velocities are concentrated at upper half of the shear box and particles are subjected to the uniform block-like motion (Figure 6d). Besides, the Figure 6d demonstrates that during shearing at the stage D to E, the particles inside the central shear zone rotate more significantly than the particles outside the shear band.

Following the formation of the shear band shows that the overall shape of the shear band is slightly curved, and deviates from the horizontal. This might be due to the non-uniform stress condition at the beginning of shearing. However, a uniform shear strain distribution both inside and outside the shear band is quite evident at the peak strength and after, indicating that progressive failure is of minor importance in a dense sample.

The 3D image of the transitional velocities of simulated sample under normal stress of 50 kPa, also shows the same trend of the formation of shear band (Figure 7).

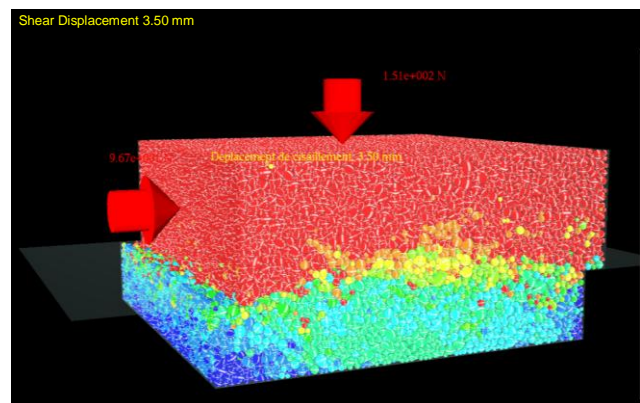


Figure 7. Post-peak transitional velocities, $\sigma_n = 50$ kPa

The total energy within the sample as the sum of the energy transfer, conversion and dissipation due to rolling and sliding of the particles were also computed for all samples. The energy results for the sample under normal stress of 50 kPa at the post-peak (Figure 8) shows that the total energy (Figure 8a) transmitted by the external forces applied on the shear box was absorbed primarily by the particles along the zero horizontal extension line due to the inter-particle friction (Figure 8b) and also particle rotations (Figure 8c). Same observation were achieved for two other simulated sample under confining stress of 200 kPa and 400 kPa. However, the magnitude of the total energy increased proportionally with the increase of the applied normal stress.

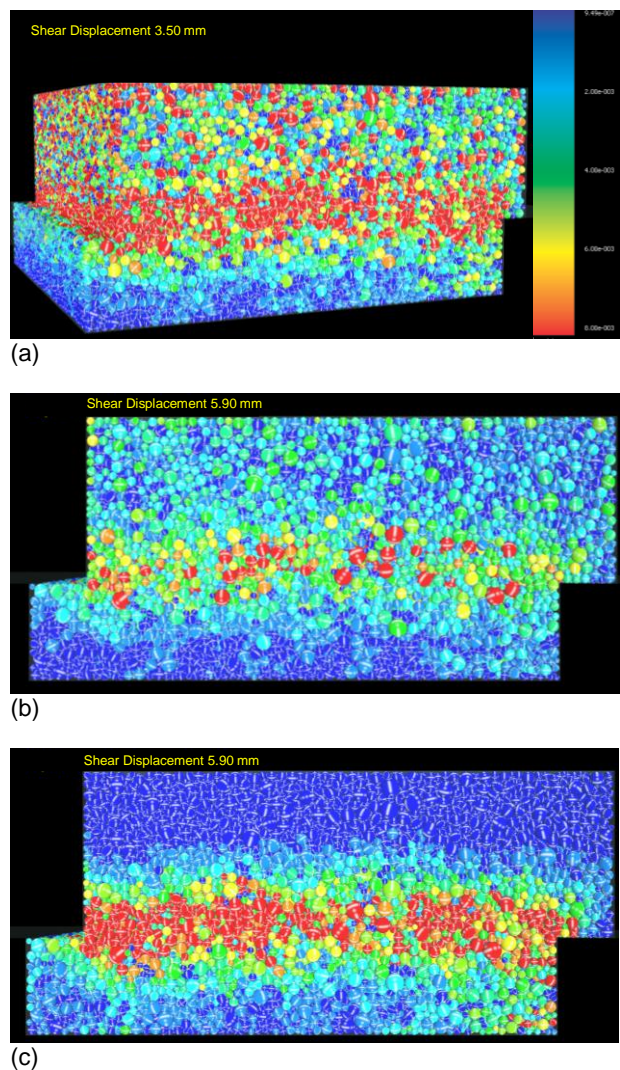


Figure 8. Computed the (a) total energy (b) frictional energy and (c) rotational energy inside the sample, under normal stress of 50 kPa at the post-peak

The simulation results here are in agreement with Numerical simulations (Pott et al. 1987, Zang and Thornton 2007) and experimental works (Dyer and Milligan, 1984, Jewell 1987) demonstrated that the high particle rotations is a significant indicator of the strain localization leading to the establishment of shear band.

4 CONCLUSION

The paper describes the DEM simulation of the samples made up of glass beads during direct shear test and under three different normal stress of 50 kPa, 200 kPa, and 400 kPa. The simulation results are compared to laboratory tests at macro-scale.

Peak and critical state data from simulations and laboratory tests are found to be in good agreement, however the rate of the dilation obtained from the

simulation do not follow the same trend as those in laboratory tests.

After validation by experimental works, the micro-scale results showing the shear band characteristics are presented.

The micro-scale results shows the initiation of strain localization from the boundaries because of the geometric constrains. The strain localization extend towards the middle of the box, while reaching the peak. Finally, during and after the peak, a distinct shear band develops along the middle plane of the box. These shear band become more continuous, concentrated and uniform while reaching the post-peak stage.

ACKNOWLEDGEMENTS

The authors would like to thank Hydro-Québec and the NSERC for their financial support throughout this research project.

5 REFERENCES

- Cundall, P. and Strack, O. 1979. A Discrete numerical model for granular assemblies. *Géotechnique* 29(1), pp. 47-65
- Cho N, Martin CD, Sego DC 2007. A clumped particle model for rock. *International Journal of Rock Mechanics and Mining Science* 44, pp. 997-1007
- Dyer MR, Milligan, G.W.E 1984. A photoelastic investigation of the interaction of a cohesionless soil with reinforcement placed at different orientations. In: *International Conference on In-Situ Soil Rock Reinforcement*, Paris, France
- Jewell, R. A. & Wroth, C. P. 1987. Direct shear tests on reinforced sand. *Géotechnique* 37(1), pp. 53-68
- Hvorslev, M. J. 1960. Physical components of the shear strength of saturated clays. *Proceedings of the research conference on shear strength of cohesive soils*, Boulder, pp. 437-501
- Morgenstern, N. R. & Tchalenko, J. S. 1967. Microscopic structure in kaolin subjected to direct shear. *Géotechnique* 17(4), pp. 309-328
- Potts, D. M., Dounias, G. T. & Vaughan, P. R. 1987. Finite element analysis of the direct shear box test. *Géotechnique* 37(1), pp. 11-23
- Roubtsova, V., Chekired, M., Karray, M., Amirpour, S. 2015. Work Energy balance for discrete element method using shear stress tests. *Congresso de Métodos Numéricos em Engenharia*, Lisboa, Portugal
- Roubtsova, V., Chekired, M., Morin, B., Karray, M. 2011. 3D Virtual Laboratory for Geotechnical Applications: Another Perspective. *International conference on particle-based methods fundamentals and applications*, Barcelona, Spain
- Terzaghi, K. & Peck, R. B. 1948. *Soil mechanics in engineering practice*. New York: Wiley
- Zhang L, Thornton C 2007. A numerical examination of the direct shear test. *Géotechnique* 57(4), pp.343-354

